

Crawling Waves Speed Estimation Based on the Dominant Component Analysis Paradigm

Ultrasonic Imaging
2015, Vol. 37(4) 341–355
© The Author(s) 2015
Reprints and permissions:
sagepub.com/journalsPermissions.nav
DOI: 10.1177/0161734614568651
ultrasonicimaging.sagepub.com


Renán Rojas¹, Juvenal Ormachea¹, Arthur Salo²,
Paul Rodríguez¹, Kevin J. Parker³, and Benjamin Castaneda¹

Abstract

A novel method for estimating the shear wave speed from crawling waves based on the amplitude modulation–frequency modulation model is proposed. Our method consists of a two-step approach for estimating the stiffness parameter at the central region of the material of interest. First, narrowband signals are isolated in the time dimension to recover the locally strongest component and to reject distortions from the ultrasound data. Then, the shear wave speed is computed by the dominant component analysis approach and its spatial instantaneous frequency is estimated by the discrete quasi-eigenfunction approximations method. Experimental results on phantoms with different compositions and operating frequencies show coherent speed estimations and accurate inclusion locations.

Keywords

Crawling wave sonoelastography, amplitude modulation–frequency modulation, dominant component analysis, quasi-eigenfunction approximations, instantaneous frequency estimation

Introduction

Elastographic imaging conveys the local biomechanical properties of soft tissue and its variations, and allows the diagnosing of pathological changes and tissue abnormalities in regions of interest.¹ While the traditional technique of evaluating such parameters is based on local palpation, its inaccuracy leads to several alternatives.² This introduces a framework consisting of external stimuli capable of causing tissue motion along with a certain imaging modality that assures a high-precision measurement.³ Imaging modalities, which include ultrasound and magnetic resonance imaging, are applied for this purpose on clinical applications such as cancer diagnosis, hepatic cirrhosis, and renal disease, among many others.⁴ Based on this, several elastographic techniques have been proposed over the last 20 years, both quantitative and qualitative,

¹Sección de Electricidad y Electrónica, Pontificia Universidad Católica del Perú, Lima, Peru

²Department of Biomedical Engineering, University of Rochester, Rochester, NY, USA

³Department of Electrical & Computer Engineering, University of Rochester, Rochester, NY, USA

Corresponding Author:

Benjamin Castaneda, Laboratorio de Imágenes Médicas, Sección de Electricidad y Electrónica, Pontificia Universidad Católica del Perú, Av. Universitaria 1801, San Miguel, Lima, 15, Peru.

Email: castaneda.b@pucp.edu.pe

which require image processing algorithms to compute viscoelastic linear and nonlinear parameter estimations and involve ill-posed inverse problems.⁵

Crawling wave sonoelastography was introduced as a method for quantifying tissue elasticity by its relation with the shear wave speed as visualized in the interference patterns of two sources oscillating at slightly different frequencies.⁶ Since its establishment, many information extraction methods have been proposed to estimate such mechanical property. Originally, Local Frequency Estimators based on the distance between interference pattern stripes were used for this task.⁶ Subsequent research included a real-time autocorrelation approach based on the local shear wave speed and its relation with the spatial derivative phase function, which allows 2-D speed estimates.⁷ Also, an overall elasticity estimation method was proposed which applied a cosine fit to a region of interest based on a cross optimization process.⁸

The crawling wave method has been successfully applied at different kinds of human tissue to characterize human skeletal muscles *in vivo*,^{9,10} human prostate tissue *ex vivo*,¹¹ and estimate human liver steatosis from dispersion estimates.^{12,13} The latter involves applying the method on highly attenuating tissues.

Clearly, the use of a model that allows an accurate computation of the interference patterns local properties is crucial for quantifying tissue stiffness. Regarding this matter, nonstationary signal modeling is currently a solid field of study applied on a wide variety of tasks. The amplitude modulation–frequency modulation (AM–FM) model allows the description of such patterns by using a sum of quasi-sinusoidal components, each characterized by an instantaneous amplitude (IA) modulation function and an instantaneous frequency (IF) modulation function, which allows a more locally coherent and well-defined frequency representation.^{14–16} The AM–FM model is a compelling way to sketch the structure of a dynamic signal as it allows to measure amplitude and oscillation rates in a local fashion. For this model, the multidimensional quasi-eigenfunction approximation (QEA) for discrete linear systems is introduced as a robust estimator of the IA and IF functions.^{17,18} Furthermore, two multi-component modeling paradigms known as dominant component analysis (DCA) and channelized component analysis (CCA) split the signal into multiple narrowband components to then associate its behavior exclusively to the locally strongest component or a sum of components, respectively.^{17,19} Overall, the AM–FM paradigm has been applied in a variety of applications, including medical purposes, with high-quality results.^{20–25}

The present work proposes the use of the AM–FM DCA model as an alternative to locally estimate the shear wave speed in the crawling waves technique by using the discrete QEA method. Prior to the demodulation task, a constraint is introduced to the ultrasound data to keep the oscillatory properties coherent with the model, which allows the rejection of spurious components that may affect the estimation accuracy. Then, the local shear wave speed is estimated by associating it to the local oscillation rate across the tissue. The rest of the document is organized as follows: the “Definition” section introduces the theoretical definitions and methods required for establishing the framework of interest, “Proposed Method” section presents the proposed method for estimating the shear wave speed from crawling waves based on the AM–FM multidimensional model, “Experimental Results” section shows the performance of the proposed method on homogeneous and nonhomogeneous phantoms, and the “Discussion” section presents a discussion regarding the theoretical and practical features of the proposed approach. Finally, “Conclusion” section presents the conclusions and future work details.

Definitions

Crawling Wave Sonoelastography

The crawling wave sonoelastography technique is built on the propagation of interference patterns inside a material via the excitation of two vibration sources. Under the plane wave

assumption and considering a homogeneous sample, the shear waves introduced by such vibration sources, expressed as W_{right} and W_{left} , can be described as follows¹¹:

$$W_{\text{right}} = e^{-\alpha(D/2+x)} e^{-i(k_1(D/2+x)-w_1t)}, \tag{1}$$

$$W_{\text{left}} = e^{-\alpha(D/2-x)} e^{-i(k_2(D/2-x)-w_2t)}, \tag{2}$$

where D is the distance between sources, α the wave attenuation factor, k_1 and k_2 the spatial frequencies, and $w_1 = 2\pi\Delta f_1$ and $w_2 = 2\pi\Delta f_2$ the vibration frequencies. In this particular case, $w = w_1 = w_2$ and $k = k_1 = k_2$. It is important to remark that both waves decay exponentially with α because they have the same spatial frequencies.

The interference patterns are the superposition of the two waves, and the corresponding squared signal envelope $|u(x, t)|^2$ is established as

$$|u(x, t)|^2 = (W_{\text{right}} + W_{\text{left}}) (W_{\text{right}}^* + W_{\text{left}}^*), \tag{3}$$

$$|u(x, t)|^2 = 2e^{-\alpha D} \{ \cosh(2\alpha x) + \cos(2kx) \}. \tag{4}$$

By using oscillation sources with slightly different frequencies (f and $f + \Delta f$ in Hz), the interference patterns will slowly move toward the source with lower frequency.⁶ In this scenario, the squared signal envelope $|u(x, t)|^2$ formed by the superposition of both waves is modeled by

$$|u(x, t)|^2 = 2e^{-\alpha D} \{ \cosh(2\alpha x) + \cos[(2k + \Delta k)x + \Delta wt] \}, \tag{5}$$

where k is the local shear wave spatial frequency, and $\Delta w = 2\pi\Delta f$ the frequency difference between the vibration sources. Focusing on the central region of the material and assuming weak wave attenuations, the hyperbolic cosine becomes constant.¹¹ By discarding the effect of this term, which represents a DC frequency component i.e. the constant value of the signal (and thus easily rejected in practical scenarios), the squared signal envelope of the interference patterns is approximated by

$$|u(x, t)|^2 \approx 2e^{(-\alpha D)} \cos[(2k + \Delta k)x + \Delta wt]. \tag{6}$$

The model establishes that the interference spatial frequency becomes approximately two times the true shear wave spatial frequency. Then, the true shear wave speed V_{shear} and the elasticity modulus E can be computed by

$$V_{\text{shear}} = \frac{2\pi \cdot f}{k}, \tag{7}$$

$$E = 3\rho(V_{\text{shear}})^2, \tag{8}$$

where f is the operating frequency and ρ the mass density of the material. Figure 1 describes the setup for the crawling waves sonoelastography technique, as well as its output data.

If Δf is small compared with f , then Δk is small compared with k . Following Equation (7), the relation between the crawling wave speed and the true shear wave speed is given as,²

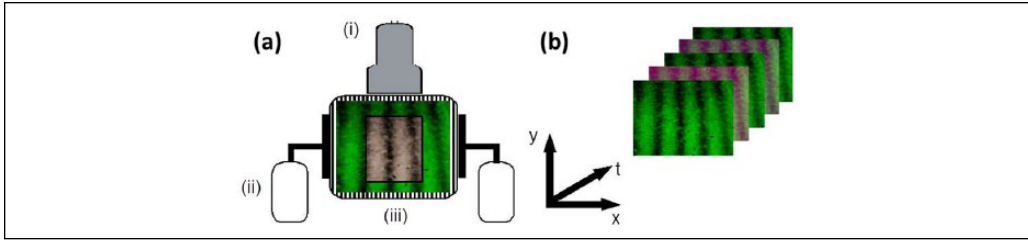


Figure 1. Ultrasound setup. (a) crawling waves sonoelastography setup, (b) ultrasound data described as a 3-D stack. (i) Ultrasound probe, (ii) mechanical sources oscillating at f and $f + \Delta f$, (iii) tissue of interest, area within the square indicates the central region.

$$V_{\text{pattern}} = \frac{\Delta w}{2w} \cdot V_{\text{shear}} \quad (9)$$

According to Equation (9), the shear waves can be “slowed down” one or two orders of magnitude by choosing $\Delta w \ll w$, so that a conventional ultrasonic scanner modified for sonoelastography can visualize and track the wave propagation. This condition will be satisfied in the experiments covered in “Experimental Results” section. In addition, the value of Δw was chosen considering a ratio of $\Delta w/f_{\text{rate}}$, where f_{rate} is the ultrasound frame rate, equal or lower than the number of samples of the slow-time signal. If this requirement is satisfied, it is possible to recover at least one period of the slow-time signal.

AM–FM

The AM–FM model represents an oscillatory signal by a sum of individual components. Its formulation is established by

$$t(x) = \sum_{i=0}^{N-1} a_i(x) \exp(j\phi_i(x)), \quad (10)$$

where each AM–FM component $t_i(x) = a_i(x) \exp(j\phi_i(x))$ is a complex-valued narrowband signal formed by an instantaneous amplitude (IA) function a_i , an instantaneous phase (IP) function ϕ_i , and an instantaneous frequency (IF) function $\nabla\phi_i$. The AM–FM components are isolated from each other on a spatio-spectrally localized basis by multiband filter banks based on Gabor functions,^{17,26} which obey design requirements to preserve coherent signal features. Refer to the literature by Bovik²⁶ and Havlicek¹⁷ for full design considerations. In practice, given a real-valued multi-component signal defined by

$$r(x) = \sum_{i=0}^{N-1} a_i(x) \cos[\phi_i(x)], \quad (11)$$

Its complex extension (analytical signal) $t(x)$ may be derived by establishing a unique imaginary part based on the Hilbert transform H as

$$t(x) = r(x) + jH(x), \quad (12)$$

$$H(x) = \sum_{i=0}^{N-1} a_i(x) \sin[\phi_i(x)]. \quad (13)$$

Following this, the signal local properties may be described by the DCA and CCA multi-component paradigms.¹⁷ DCA models the signal’s nonstationary behavior at each x coordinate by exclusively taking into account the AM–FM component with the strongest response, also known as the AM–FM dominant component, which corresponds to the isolated signal with the highest signal-to-noise ratio. However, CCA builds a multi-component description based on the sum of multiple AM–FM components at each x coordinate. Although the latter model includes more compelling signal information, it may also include components that contain exclusively noise elements, which may lead to an inaccurate signal representation. Regarding the DCA, the AM–FM dominant component is defined at each x coordinate by the channel response that maximizes the following channel selection criterion^{17,19}:

$$\Psi_m(x) = \frac{y_m(x)}{\max_{\Omega} |G_m(\Omega)|}, \tag{14}$$

where m indicates the channel, $y_m(x)$ the channel response at x , and $G_m(\Omega)$ the filter response at frequency Ω .

To estimate the instantaneous amplitude and IF functions, a demodulation method is required. Among the existing methods, the discrete QEA approach allows an accurate estimation for discrete signals and successfully locates the estimated frequencies in the interval $[-\pi, \pi]$.¹⁷ AM–FM modulating functions based on the QEA method are computed as follows:

$$e_i \nabla \hat{\varphi}(x) = \sin^{-1} \left[\frac{y(x+e_i) - y(x-e_i)}{2jy(x)} \right] = \cos^{-1} \left[\frac{y(x+e_i) + y(x-e_i)}{2y(x)} \right], \tag{15}$$

$$\hat{a}(x) = \left| \frac{y(x)}{G[\nabla \hat{\varphi}(x)]} \right|, \tag{16}$$

where e_i is a unit vector with direction i , y is a narrowband complex signal, and G the filter amplitude.

Proposed Method

Pre-processing Procedure

Equation (6) provides a way to analyze the interference patterns at specific frames and lateral distance coordinates, which are denoted by t and x , respectively. For a fixed x coordinate, it is straightforward to verify that the pattern follows a sinusoidal function along t . As expected, this may not hold in practical scenarios where ultrasound data include noise components. Thus, recovering the original patterns becomes an ill-posed inverse problem that can be dealt with by using the AM–FM approach.

Following this, a more accurate representation of the interference patterns is obtained prior to estimating the local shear wave speed. First, a 7×3 median filter is applied at each ultrasound frame.¹¹ Then, the AM–FM dominant component along t for every lateral distance x is extracted from the ultrasound data. Assuming that the strongest AM–FM component corresponds to the interference patterns while the rest of components correspond to noise content, the AM–FM dominant component along t for a lateral coordinate x_0 corresponds to $|u(x_0, t)|^2$. For this function, the phase argument $(2k + \Delta k)x_0$ is of particular interest because it contains information about the local shear wave spatial frequency, while the frequency argument corresponds to $\Delta\omega$.

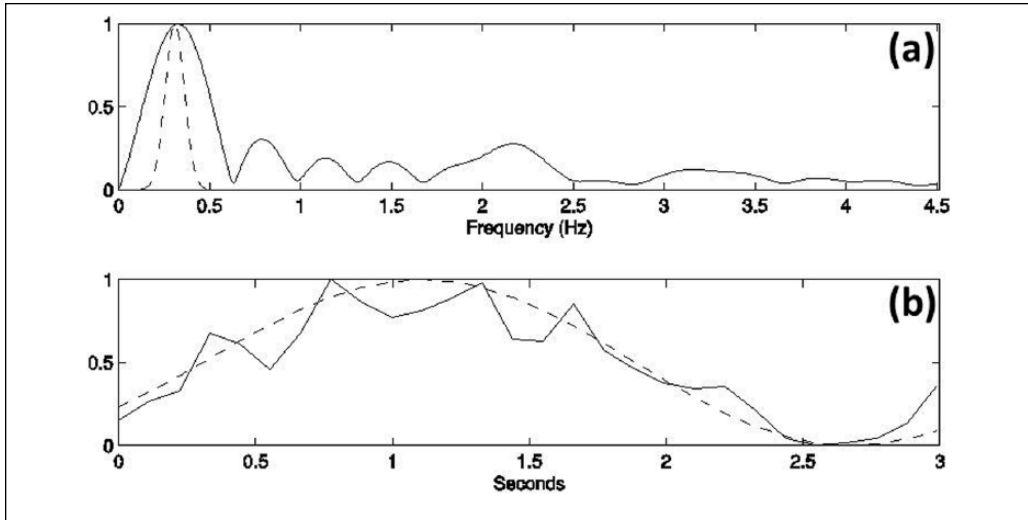


Figure 2. Dominant component recovery along t . Normalized for display purposes. (a) Original signal frequency components vs. dominant channel response (dotted line), (b) original signal vs. dominant signal (dotted line).

Narrowband components are isolated by applying a well spectrally localized 30-channel unit-L2 norm Gabor filterbank along t . The filterbank is designed to cover a frequency domain from zero to half the frame rate, which depends on the ultrasound setup. It is important to note that the goal here is not to demodulate the AM–FM dominant component but to reject the rest of components to remove spurious elements from the ultrasound data.

Shear Wave Speed Estimation Procedure

With the noise content attenuated by the previous procedure, an accurate estimation of the local shear wave spatial frequency is required to compute the local speed, as established by Equation (7). This is achieved by using the AM–FM model along the lateral dimension. To avoid the presence of noise components that were not fully attenuated by the pre-processing approach and assuming the strongest AM–FM component still corresponds to the interference patterns, the DCA paradigm is applied. Thus, the dominant component along x for a frame t_0 corresponds to $|u(x, t_0)|^2$ and its IF function corresponds to the frequency argument $(2k + \Delta k)$. As Δk is much less than k , the IF function becomes twice the local shear wave spatial frequency.¹¹

A 6-channel unit-L2 norm Gabor filterbank with half-peak radial bandwidths of 1.5 octaves and 1.5 common ratio ($r_0 = 1 \text{ cm}^{-1}$) is used for the narrowband signal isolation.¹⁷ IF estimates are then computed for each channel using the QEA method.

Shear wave speed computations are performed once the IF at each frame is estimated via the QEA method. For this purpose, the effective IF at each point is established as its median value computed across all frames. Figures 2 and 3 describe the pre-processing stage for a fixed lateral distance x_0 and the demodulation approach for a specific frame t_0 , respectively.

Experimental Results

The performance of the proposed method is evaluated on a set of three homogeneous phantoms with varying gelatin content and a set of four inclusion (nonhomogeneous) phantoms with

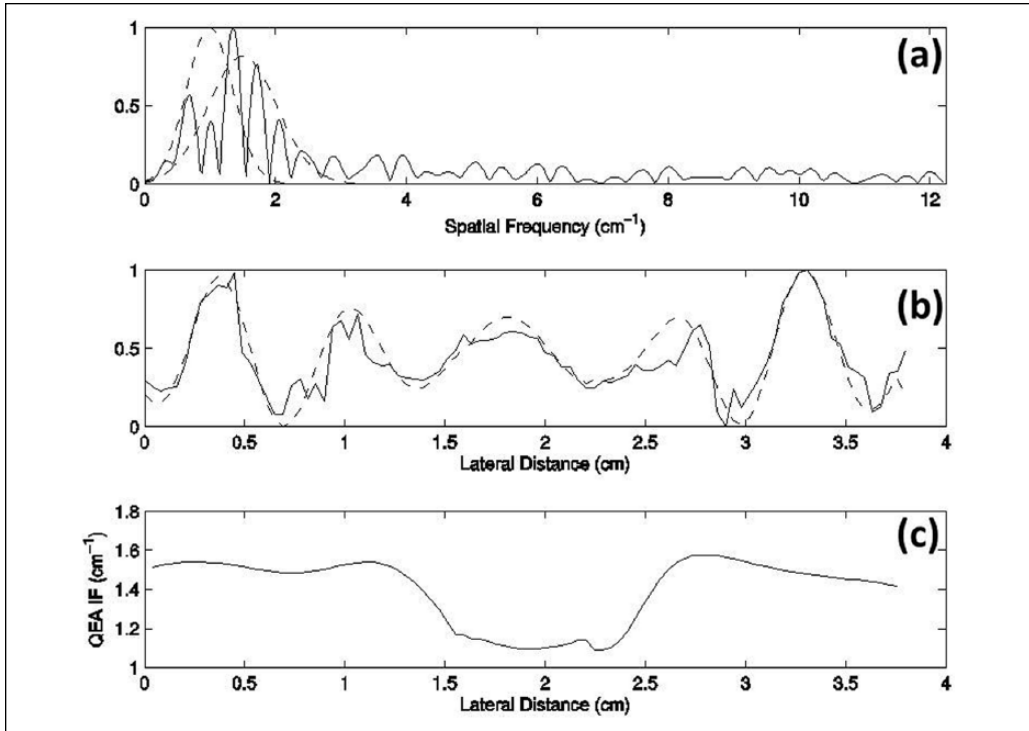


Figure 3. DCA along x ($\Delta f = 0.35$ Hz). Normalized for display purposes. (a) Pre-processed signal frequency components vs. dominant channels response (dotted line), (b) pre-processed signal vs. DCA output (dotted line), (c) QEA instantaneous frequency (IF) estimation. DCA = dominant component analysis; QEA = quasi-eigenfunction approximation.

inclusions of varying diameter. Table 1 describes the phantom set composition. The crawling waves setup includes operating frequencies that cover from 140 Hz to 360 Hz in steps of 20 Hz. Table 2 describes the equipment used in the crawling waves experiments. The ultrasound data collection parameters are as follows. Doppler frequency: 5 MHz, central frequency: 7.5 MHz, frame rate: between 9.03 Hz and 10.11 Hz.

The pre-processing approach performance is classified by the dominant component frequency and its contrast with $\Delta\omega$, which is known from the experimental setup, for three inclusion (non-homogeneous) phantoms and three homogeneous phantoms at each operating frequency. The local speed estimation performance is classified by its comparison against mechanical measurements for the homogeneous set and by the inclusion localization and inclusion-background contrast based on B-mode data for the inclusion set.

Pre-processing

The dominant component extraction performance is examined. Figures 4 and 5 describe a comparison between the original signal, its median filtering output, and the proposed approach for the homogeneous phantom and inclusion phantom cases, respectively. The proposed approach consists of a median filtering plus the AM-FM dominant component isolation. The comparison is made at 240 Hz operating frequency and $\Delta f = 0.35$ Hz, and shows a considerable improvement in the signal behavior as compared with exclusively applying a median filter. Figure 6 shows the

Table 1. Phantom Set Composition.

		Degassed water (ml)	NaCl ^a (g)	Gelatin ^b (g)	Graphite ^c (g)
Nonhomogeneous	Inclusion (16% gelatin)	150	1.35 (0.9%)	28.57	18 (12%)
	Background (10 % gelatin)	1800	16.2 (0.9%)	200	36 (2%)
Homogeneous	10% gelatin	1800	16.2 (0.9%)	200	36 (2%)
	13% gelatin	1800	16.2 (0.9%)	269	36 (2%)
	16% gelatin	1700	15.3 (0.9%)	323.8	36 (2.1%)

^aPercentages based on the water content.

^bGelatin information: 300 Bloom Type A pork 40 mesh. Percentages based on the water plus gelatin content.

^cGraphite information: Powder G67-500. Percentages based on the water content.

Table 2. Ultrasound Equipment Used in the Crawling Waves Experiments.

Equipment	Model and manufacturer
Amplifier	5530, AE Techron (USA)
Dual channel function generator	AFG3022B, Tektronix (USA)
Mechanical vibration sources	Brüel & Kjaer, Naerum (Denmark)
Ultrasound system	GE Logiq 9, GE Healthcare (USA)
Linear array ultrasound transducer	M12L, GE Healthcare (USA)

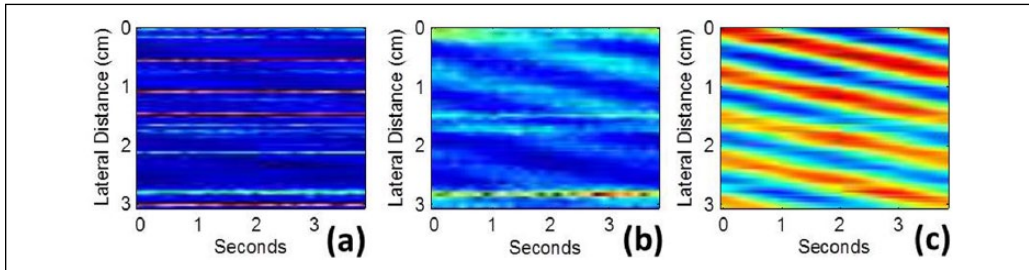


Figure 4. Pre-processing results for a homogeneous phantom ($f = 240$ Hz). (a) Original data, (b) median filtering output, (c) proposed approach: median filtering plus dominant component extraction.

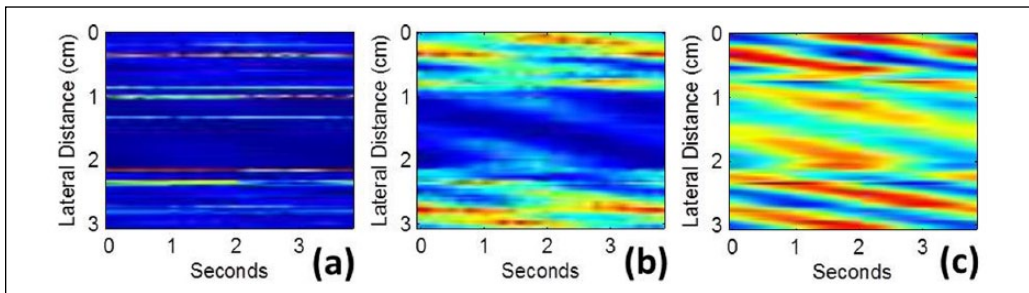


Figure 5. Pre-processing results for an inclusion phantom ($f = 240$ Hz). (a) Original data, (b) median filtering output, (c) proposed approach: median filtering plus dominant component extraction.

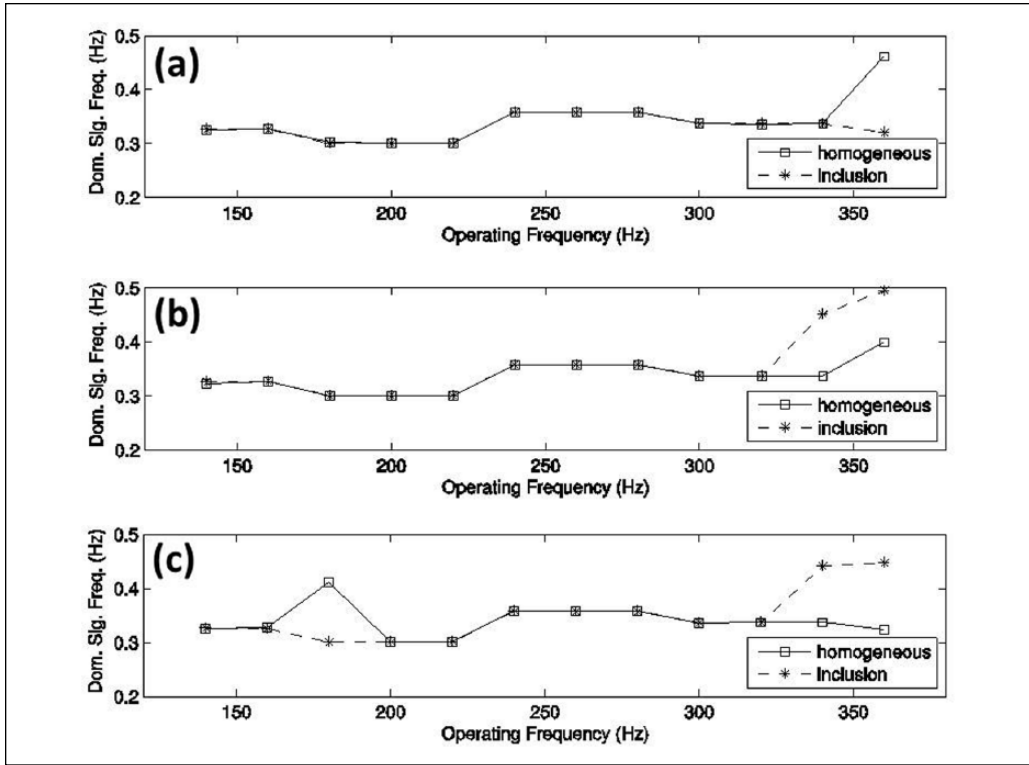


Figure 6. Frequency mean for the estimated dominant signal from homogeneous (blue) and inclusion (red) phantoms ($\Delta f = 0.35$ Hz). (a) 10% gelatin phantom vs. $\phi = 1.83$ cm diameter inclusion phantom, (b) 13% gelatin phantom vs. $\phi = 1.35$ cm diameter inclusion phantom, (c) 16% gelatin phantom vs. $\phi = 0.68$ cm diameter inclusion phantom.

IF means for the dominant signal for each test phantom at each operating frequency and $\Delta f = 0.35$ Hz. Standard deviations for all cases are below 10^{-14} . Results show that the dominant frequency is close to $\Delta\omega$ in most cases, which is consistent with the crawling waves model.

Speed Estimation for Homogeneous Phantoms

Spatial frequency estimations based on the proposed method are presented for homogeneous phantoms. Figure 7 shows the estimated shear wave average speed and standard deviation for 10%, 13%, and 16% gelatin phantoms, along with the corresponding mechanical measurements. Both statistical properties were computed from a rectangular region with one-third the width and height of the frame and located at its center. The average speed v_m and standard deviation v_{sd} were computed as follows:

$$v_m = \frac{1}{N} \sum_{i=0}^{N-1} v_i, \tag{17}$$

$$v_{sd} = \sqrt{\frac{1}{N} \sum_{i=0}^{N-1} (v_i - v_m)^2}. \tag{18}$$

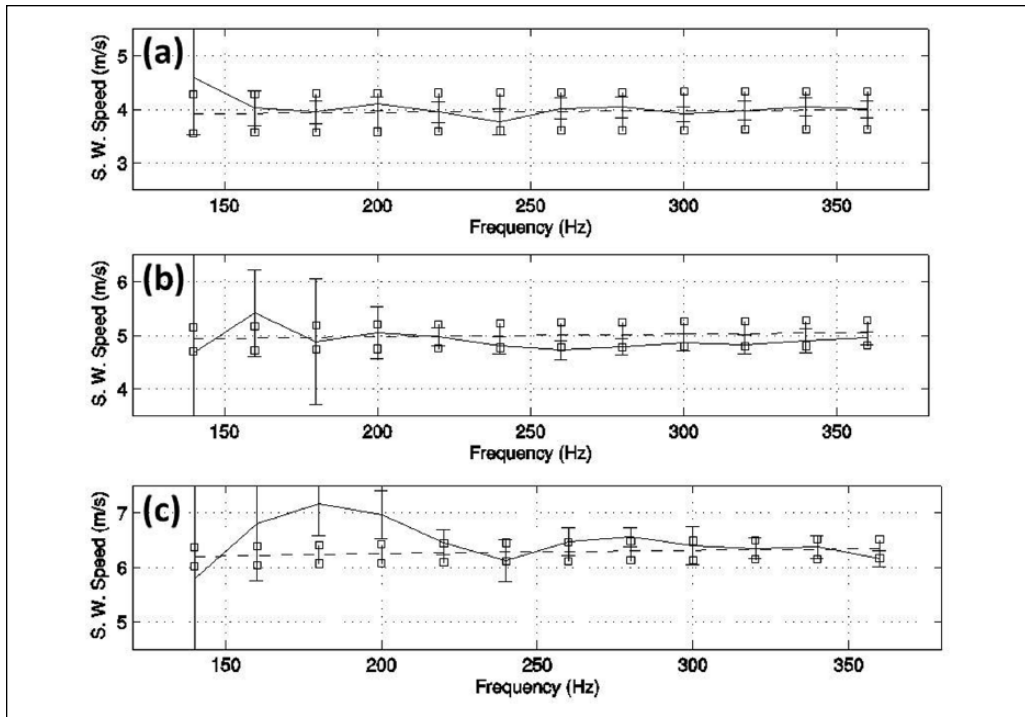


Figure 7. Shear wave average speed and standard deviation contrast between the proposed method and mechanical measurements (dotted line) for inclusion phantoms. (a) 10% gelatin phantom, (b) 13% gelatin phantom, (c) 16% gelatin phantom.

The average speed is relatively accurate for all three cases, especially for operating frequencies above 200 Hz. For lower operating frequencies, the average speed becomes slightly less accurate for the 10% and 13% gelatin phantoms, while considerably less accurate for the 16% gelatin phantom. The largest average speed error for the 10% gelatin phantom is at 160 Hz (0.67 m/s), for the 13% gelatin phantom is at 140 Hz (0.47 m/s), and for the 16% gelatin phantom is at 180 Hz (0.93 m/s). The estimated speed standard deviation presents the lowest values for operating frequencies above 200 Hz in all three cases. Also for all three cases, the standard deviation at 140 Hz is the largest with 0.24 m/s for the 10% gelatin phantom, 0.32 m/s for the 13% gelatin phantom, and 1.88 m/s for the 16% gelatin phantom. For display purposes, the shear wave speed range on Figure 7 does not include the standard deviations for all operating frequencies.

The previous observations clearly show a strong relation between the speed estimation accuracy and two main features: (a) the gelatin content of the phantom, which implies the stiffness of the material and (b) the operating frequency, which is directly associated to the local shear wave spatial frequency k by Equation (7). Both the increase of gelatin content (i.e., stiffer materials) and the decrease of the operating frequency lead to a less accurate speed estimation because the resulting shear wave is characterized by a low local spatial frequency, and thus the ultrasound data may not include enough information for an adequate reconstruction.

Speed Estimation for Inclusion Phantoms

Spatial frequency estimations based on the proposed method are presented for inclusion phantoms. Figures 8 and 9 show the estimated shear wave speed based on the proposed method for

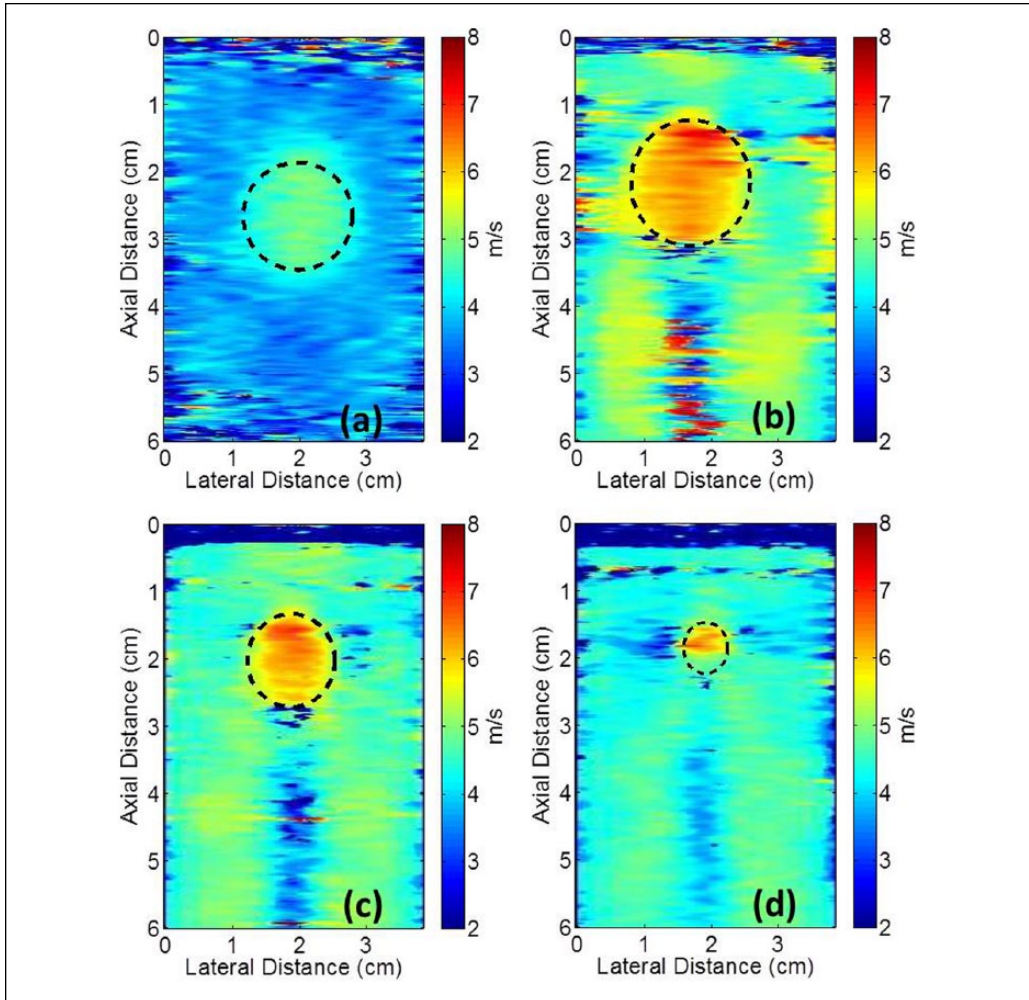


Figure 8. Shear wave speed estimation images for the inclusion phantom set at 340 Hz operating frequency. The dotted regions describe the inclusion size and their respective diameters (ϕ) based on B-mode images information. (a) $\phi = 1.54$ cm inclusion ($\Delta f = 0.4$ Hz), (b) $\phi = 1.83$ cm inclusion ($\Delta f = 0.35$ Hz), (c) $\phi = 1.35$ cm inclusion ($\Delta f = 0.35$ Hz), (d) $\phi = 0.68$ cm inclusion ($\Delta f = 0.35$ Hz).

four different inclusion diameters at 340 Hz operation frequency and its contrast with B-mode images, respectively. Specifically, the evaluation covers the following inclusion diameters: 1.54 cm (at $\Delta f = 0.4$ Hz), 1.83 cm (at $\Delta f = 0.35$ Hz), 1.35 cm (at $\Delta f = 0.35$ Hz), and 0.68 cm (at $\Delta f = 0.35$ Hz). Results show that high local shear wave speed corresponding to inclusion regions is correctly localized for all cases.

However, there is a considerable amount of artifacts that reduces the contrast between inclusion and homogeneous regions. Specifically, due to the shadowing effects shown in the B-mode images included in Figure 9, the crawling waves images include artifacts located below the inclusions. This causes a lack of accurate IQ signals at such regions and subsequent inaccurate speed estimations, as shown in Figure 8. From the four described scenarios, the one with the smallest inclusion diameter (0.68 cm) shows the most inaccurate localization.

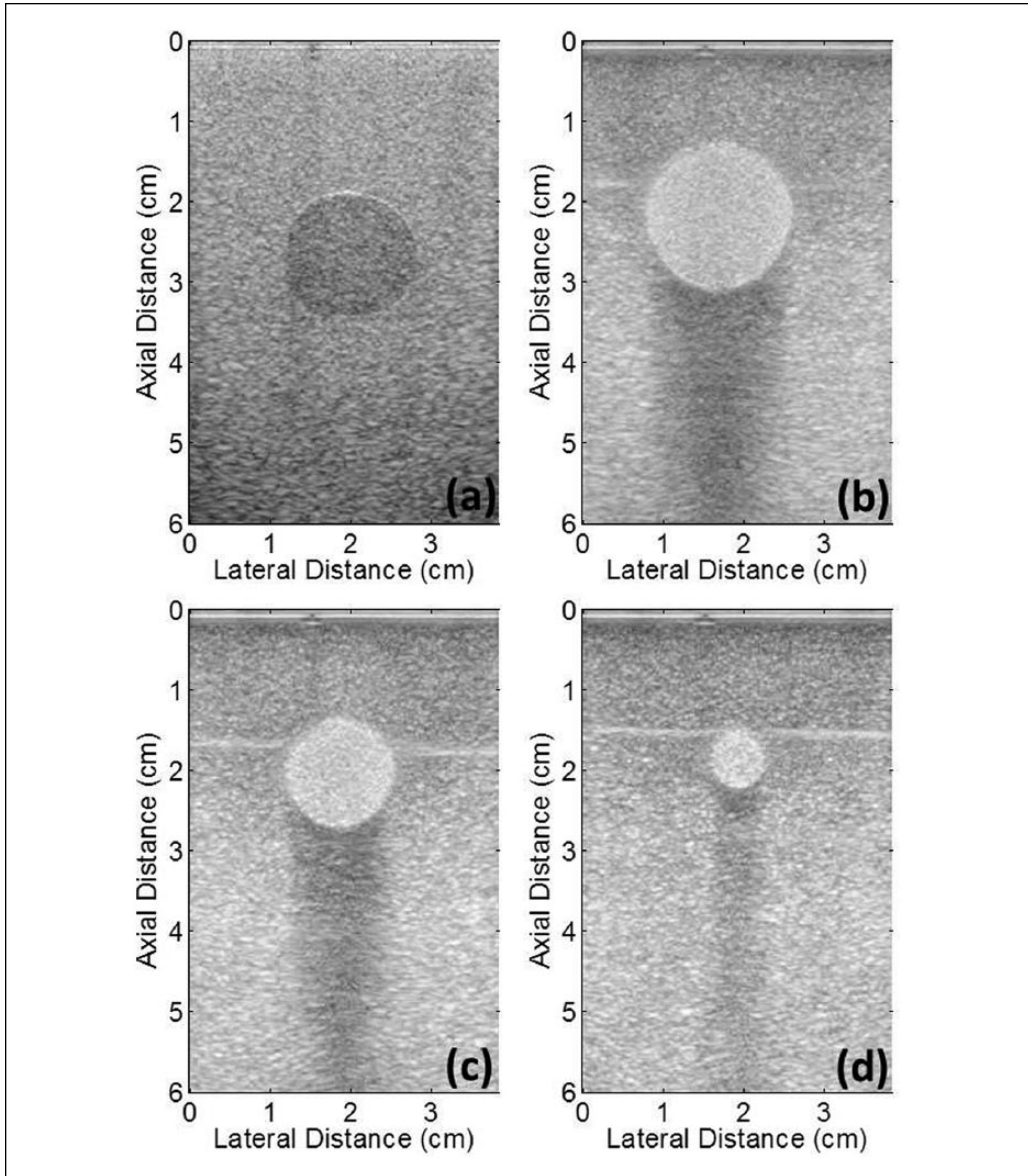


Figure 9. B-mode images for the inclusion phantom set at 340 Hz operating frequency. (a) $\phi = 1.54$ cm inclusion ($\Delta f = 0.4$ Hz), (b) $\phi = 1.83$ cm inclusion ($\Delta f = 0.35$ Hz), (c) $\phi = 1.35$ cm inclusion ($\Delta f = 0.35$ Hz), (d) $\phi = 0.68$ cm inclusion ($\Delta f = 0.35$ Hz).

Discussion

While the main contribution of the proposed method is the use of the AM–FM framework for estimating tissue elasticity, a crucial step for achieving this lies in its noise rejection procedure that isolates the dominant component along frames from the ultrasound data. As there is no extensive study in the literature regarding the ultrasound noise distribution under the scenario of interest, the efficiency of such a method is based on the premise that the strongest AM–FM

component corresponds to the crawling waves, rather than in any a priori information about the noise properties.

Another potential source of error is the presence of reflected shear wave components at boundaries. The impact of any reflected waves is greatest near boundaries and may affect local shear wave speed estimation, especially at low frequencies. However, as the attenuation coefficient increases with frequency, reflections are rapidly attenuated for high frequencies and their impact in the speed estimation is minimized.

However, the crawling waves model adopted in this research is a simplified version of the general model valid exclusively in the central region and under weak wave attenuation, as established in the “Definitions” section. While the original research included the general superposition pattern, this was abandoned for one main reason: the introduction of the $\cosh(2ax)$ component imposes the requirement to compute the wave attenuation factor a to estimate k . As a consequence, the research focused exclusively on demonstrating the benefits of the AM–FM model under the aforementioned conditions as an initial step toward a general framework.

Another important assumption in the estimation technique is a planar shear wave propagation. Although this assumption might not hold for nonhomogeneous material such as the inclusion phantoms evaluated in the experiments, it was adopted as an initial step toward demonstrating the potential of the AM–FM technique. Unquestionably, nonhomogeneous phantoms will show shear waves that deviate from plane wave conditions, and in that sense, the proposed estimation method is biased. Nonetheless, the experiments show accurate inclusion localizations and give enough motivation to extend the use of AM–FM to a multidimensional shear wave speed model that provides better results, such as similar approaches in the literature.⁷

Conclusion

A novel method for estimating the local shear wave speed from crawling waves sonoelastography is proposed based on the AM–FM framework. To reject signal distortions, a pre-processing approach to reject the nondominant components along frames is applied to the ultrasound data. Following this, the local shear wave speed is computed by estimating the IF function along the lateral direction based on the DCA multi-component model. Experimental results on homogeneous phantoms show that the estimation accuracy varies for different oscillation frequencies, while experimental results for inclusion phantoms show consistent inclusion localizations with a low contrast between inclusions and homogeneous regions. Based on the latter, the use of this method requires improvement to be applied in medical tasks where precise quantification of small lesions is required.

Future work will focus on three aspects. First, an in-depth study of the noise distribution in the ultrasound data will be carried out to define an adequate restoration procedure. Second, a comprehensive review of alternative filter types that improve the preservation of the isolated signal properties will be performed. Third, an improvement of the estimation method will be proposed to compute multidimensional speed estimations and extend its application to different modalities such as magnetic resonance elastography (MRE).

Declaration of Conflicting Interests

The author(s) declared no potential conflicts of interest with respect to the research, authorship, and/or publication of this article.

Funding

The author(s) disclosed receipt of the following financial support for the research, authorship, and/or publication of this article: This work was supported by the Peruvian Science and Technology Program (FINCyT), contract No. 205-FINCyT-IA-2013.

References

1. Parker KJ, Taylor LS, Gracewski S, Rubens DJ. A unified view of imaging the elastic properties of tissue. *J Acoust Soc Am.* 2005;117(5):2705–12.
2. Wu Z. Shear wave interferometry and holography, an application of sonoelastography. PhD thesis, University of Rochester, 2005.
3. Ophir J, Cespedes I, Ponnekanti H, Yazdi Y, Li X. Elastography: a quantitative method for imaging the elasticity of biological tissues. *Ultrason Imaging.* 1991;13(2):111–34.
4. Parker KJ, Doyley M, Rubens D. Imaging the elastic properties of tissue: the 20 year perspective. *Phys Med Biol.* 2011;56(1):R1–29.
5. Castaneda B, Ormachea J, Rodriguez P, Parker KJ. Application of numerical methods to elasticity imaging. *Mol Cell Biomech.* 2013;10(1):43–65.
6. Wu Z, Taylor LS, Rubens DJ, Parker KJ. Sonoelastographic imaging of interference patterns for estimation of the shear velocity of homogeneous biomaterials. *Phys Med Biol.* 2004;49(6):911–22.
7. Hoyt K, Castaneda B, Parker KJ. Two-dimensional sonoelastographic shear velocity imaging. *Ultrasound Med Biol.* 2008;34(2):276–88.
8. Zhang M, Castaneda B, Wu Z, Nigwekar P, Joseph JV, Rubens DJ, Parker KJ. Congruence of imaging estimators and mechanical measurements of viscoelastic properties of soft tissues. *Ultrasound Med Biol.* 2007;33(10):1617–31.
9. Hoyt K, Castaneda B, Parker KJ. 5C-6 muscle tissue characterization using quantitative sonoelastography: preliminary results. In: *Ultrasonics Symposium*, New York, NY, 28–31 October 2007, pp. 365–68.
10. Hoyt K, Kneezel T, Castaneda B, Parker KJ. Quantitative sonoelastography for the in vivo assessment of skeletal muscle viscoelasticity. *Phys Med Biol.* 2008;53(15):4063–80.
11. Castaneda B, An L, Wu S, Baxter LL, Yao JL, Joseph JV, et al. Prostate cancer detection using crawling wave sonoelastography. *SPIE Medical Imaging.* 2009; 7265:1–10.
12. Barry CT, Mills B, Hah Z, Mooney RA, Ryan CK, Rubens DJ, et al. Shear wave dispersion measures liver steatosis. *Ultrasound Med Biol.* 2012;38(2):175–82.
13. Barry CT, Hah Z, Partin A, Mooney RA, Chuang KH, Augustine A, et al. Mouse liver dispersion for the diagnosis of early-stage fatty liver disease: a 70-sample study. *Ultrasound Med Biol.* 2014;40(4): 704–13.
14. Maragos P, Bovik AC. Image demodulation using multidimensional energy separation. *JOSA A.* 1995;12(9):1867–76.
15. Havlicek JP, Harding DS, Bovik AC. Reconstruction from the multi-component AM-FM image representation. In: *Proceedings of International Conference on Image Processing*, Washington, DC, 23–26 October 1995, 2:280–3.
16. Lu S, Doerschuk PC. Nonlinear modeling and processing of speech based on sums of AM-FM formant models. *IEEE Trans Signal Process.* 1996;44(4):773–82.
17. Havlicek JP. AM-FM image models. PhD thesis, University of Texas at Austin, 1996.
18. Havlicek JP, Harding DS, Bovik AC. Discrete quasi-eigenfunction approximation for AM-FM image analysis. In: *Proceedings of International Conference on Image Processing*, Lausanne, Switzerland, 16–19 September 1996, 1:633–36.
19. Havlicek JP, Harding DS, Bovik AC. Multidimensional quasi-eigenfunction approximations and multicomponent AM-FM models. *IEEE Trans Imag Process.* 2000;9(2):227–42.
20. Murray V, Barriga ES, Soliz P, Pattichis MS. Survey of AM-FM methods for applications in medical imaging. *Ibero-American Conference on Trends in Engineering Education and Collaboration (CITECI)*, Albuquerque, NM, 27–28 October 2009. Available from http://www.istec.org/wp-content/gallery/ebooks/citeci/docs/final_citeci.pdf.
21. Pattichis MS, Pattichis CS, Avraam M, Bovik A, Kyriacou K. AM-FM texture segmentation in electron microscopic muscle imaging. *IEEE Trans Med Imaging.* 2000;19(12):1253–57.
22. Elshinawy MY, Zeng J, Lo SC, Chouikha MF. Breast cancer detection in mammogram with AM-FM modeling and Gabor filtering. In: *Proceedings of 7th International Conference on Signal Processing*, ICSP'04, Beijing, China, 31 August–4 September 2004, 3:2564–67.

23. Rodriguez P, Pattichis M. Nested random phase sequence sets: a link between AM-FM demodulation and increasing operators with application to cardiac image analysis. In: 6th IEEE Southwest Symposium on Image Analysis and Interpretation, Lake Tahoe, NV, 28–30 March 2004, pp. 196–200.
24. Murray V, Rodriguez P, Pattichis MS. Multiscale AM-FM demodulation and image reconstruction methods with improved accuracy. *IEEE Trans Imag Process.* 2010;19(5):1138–52.
25. Rodriguez P, Pattichis MS, Goens MB. M-mode echocardiography image and video segmentation based on AM-FM demodulation techniques. In: Proceedings of the 25th Annual International Conference of the IEEE Engineering in Medicine and Biology Society, Cancun, Mexico, 17–21 September 2003, 2:1176–79.
26. Bovik AC. *Handbook of Image and Video Processing.* Elsevier Academic Press, San Diego, CA, 2nd edition, 2005.